Accepted to the Astrophysical Journal

Magnetic Fields in Quasar Cores

Gregory B. Taylor
National Radio Astronomy Observatory, Socorro, NM 87801, USA

ABSTRACT

Multi-frequency polarimetry with the Very Long Baseline Array (VLBA) telescope has revealed absolute Faraday Rotation Measures (RMs) in excess of 1000 radians m^{-2} in the central regions of the quasars 3C 273, 3C 279 and 3C 380. Beyond a projected distance of $\sim$20 h^{-1} pc, however, the jets of all three sources are found to have |RM| < 100 radians m^{-2}. Such sharp RM gradients cannot be produced by cluster or galactic-scale magnetic fields, but rather must be the result of magnetic fields organized on scales of 1–100 pc. If associated with the region that produces the narrow optical emission lines, then magnetic fields of strength $\sim$0.05 μG are required to be uniform over scales of $\sim$10 pc. The direct detection of high RMs in these quasar cores can explain the low fractional core polarizations usually observed in quasars at centimeter wavelengths as the result of irregularities in the Faraday screen on scales smaller than the telescope beam.

Subject headings: galaxies:active — galaxies: jets — radio continuum: galaxies — galaxies:ISM — galaxies: nuclei

1. Introduction

The parsec-scale cores and jets of quasars have typical linear polarizations of 1-10% (Cawthorne et al. 1993) with the jets being more strongly polarized. The electric field polarization angle of the jet has been found to be generally perpendicular to the jet axis (Roberts et al. 1989). In the case of optically thin synchrotron emission this implies a projected magnetic field aligned in parallel with the jet direction. The polarization angle of the core component does not seem to correlate with source structure, although for 3C 345 and 3C 279 Leppänen, Zensus & Diamond (1995) have postulated a magnetic field which changes from transverse to longitudinal from the core to the jets due to strong plane-perpendicular shocks in the jets.

Until recently measurements of the magnetic field orientation in quasars (e.g. Cawthorne et al. 1993) have been assumed to have negligible Faraday Rotation (which turns the polarization angle in proportion to λ^2), or to have a constant Rotation Measure (RM) equal to the integrated RM measured by the VLA or single dish telescopes. This situation arose from the difficulty in obtaining the simultaneous, multi-frequency VLBI polarimetry needed to determine the RM on the parsec-scale. Recent observations of OQ 172 by Udomprasert et al. (1997) and 3C 138 by Cotton et al. (1997) have revealed high RMs in the nuclei of these two quasars. To further investigate the parsec-scale RM distribution in quasars I have performed multi-frequency polarimetric observations of 4 strong quasars using the VLBA. These sources were chosen by virtue of their strength, presence of known extended polarized flux, and scheduling restrictions. This selection was made more to demonstrate the technique of measuring RMs on the parsec-scale than to try to constitute a complete sample.

I assume H_0 = 50 km s^{-1} Mpc^{-1} and q=0.5 throughout.

2. Observations

2.1. Data Reduction Procedures

The observations, performed on 1997 Jan. 25 (1997.07), were carried out at multiple frequencies (or IFs) between 4.6 and 15.2 GHz (see Table 1) using the 10 element VLBA.[1] Both right and left circular polarizations were recorded using 1 bit sampling across a bandwidth of 8 MHz. The VLBA correlator produced 16 frequency channels across each IF during every 2 second integration.

Amplitude calibration for each antenna was derived from measurements of the antenna gain and system temperatures during each run. The polarization calibration was performed following a procedure suggested by Cotton (1993). Global fringe fitting was performed using the AIPS task FRING, an implementation of the Schwab & Cotton (1983) algorithm. The fringe fitting was performed on each IF and polarization independently using a solution interval of 2 minutes, and a point source model was assumed. Next, a short segment of the cross hand data from the strongly polarized calibrator 3C 273 was fringe fitted in order to determine the right-left delay difference, and the correction obtained was applied to the rest of the data. Once delay and rate solutions were applied the data were averaged in frequency over 8 MHz. The data from all sources were

[1]The National Radio Astronomy Observatory is operated by Associated Universities, Inc., under cooperative agreement with the National Science Foundation

edited and averaged over 30 second intervals using DIFMAP (Shepherd, Pearson & Taylor 1994, 1995) and then were subsequently self-calibrated using AIPS and DIFMAP in combination.

Next, the strong, compact calibrator J1640+397 was used to determine the feed polarizations of the antennas using the AIPS task PCAL. I assumed that the VLBA antennas had good quality feeds with relatively pure polarizations, which allowed us to use a linearized model to fit the feed polarizations. Once these were determined, the solutions were applied to snapshot observations of the compact sources J0818+423 and J1800+784. These two sources (and the program sources) were observed with the VLA on 1997 January 28. The flux density scale and polarization angle calibration at the VLA were set using 3C 286. Good agreement was found between the polarized flux densities measured with the VLA and VLBA (see Table 2), and the VLA polarization angles were used to determine appropriate corrections to the VLBA polarization angles. These corrections were found in general to be small within the VLBA bands ($<10°$), but significant between bands.

2.2. Reliability

The absolute electric vector polarization angle calibration procedures outlined above could introduce an error in the measured polarization angles at each frequency of up to $\sim3°$. A $3°$ rotation in polarization angle between observations at 8 and 15 GHz, the frequency range primarily used here for RM determinations, corresponds to a RM of 50 radians m^{-2}. Between 5 and 8 GHz the RM due to absolute calibration errors is $\sim$25 radians m^{-2}. Note, however, that this error will be constant over all sources, and as such will not affect the differences in RM found in a given source.

Errors in the polarization calibration of the antenna feeds will translate into errors in the polarization images. Roberts et al. (1994) estimate that the feed terms can usually be determined to an accuracy of $<0.5\%$. For alt-azimuth mounted antennas this leads to a noise in the polarized intensity of $\sim0.1\%$ of the peak in the total intensity image. The method of polarization calibration introduced by Leppänen et al. (1995), is found to give similar errors. For sources like 3C 279 with peaks in stokes I of $\sim$10 Jy this translates to an error in Stokes Q and U of $\sigma_{\rm P} \sim 10$ mJy. Another source of error results from the incomplete sampling in the uv-plane and the consequent deconvolution errors. For the strong, complicated sources presented here, the deconvolution errors will dominate over the random errors due to thermal noise, and that from errors in the polarization calibration. I have tried to estimate the impact of the deconvolution errors by measuring the peak polarized signals off-source. I interpret these non-physical features where the polarized intensity exceeds the total intensity, as $2\sigma_{\rm P}$ fluctuations. This estimate for $\sigma_{\rm P}$ ranges from a factor of 2–5 larger than that estimated by the thermal noise alone. The corresponding errors in the polarization angles are typically $\sim2°$, comparable with those quoted by others (e.g. Brown, Roberts & Wardle 1994).

3. Results

In order to compare images of the total intensity, polarized intensity, and polarization angle obtained at different frequencies with a fixed array of antennas, it is necessary to taper the observations made at higher frequencies (and hence higher intrinsic resolution) in order to match the resolution of the lowest frequency observed. Various combinations of images were produced covering the ranges from 5-8 GHz, 8-15 GHz, and 12-15 GHz. The heavy taper required to match the 15 GHz to the 5 GHz resolution made this combination of limited utility. And as the cores were generally found to depolarize at 5 GHz, most of the results presented here have been derived from the 7 frequencies in the range 8–15 GHz (see Table 1). Faraday Rotation Measures were obtained by performing a least-squares fit of a λ^2-relation to measurements of the polarization angle at each pixel in matched-resolution images.

In the process of fringe-fitting the VLBA data, the brightest component of each source (in all cases the flat-spectrum core component) is shifted to the map center. If this core component is the location in the jet where the synchrotron self absorption optical depth is unity, then its position will vary with frequency (Blandford & Königl 1979), such that higher frequencies look "deeper" down the jet towards the true center of activity. This frequency dependent shift of the core component can be measured by using optically thin features in the jet to register simultaneous, multi-frequency observations (see e.g. Lobanov 1996). The amount of this shift is small, < 0.2 mas between 5 and 15 GHz for 3C 345 (Lobanov 1996). For all the observations presented here, the registration of the multi-frequency observations were found to be within 10% of the beam size, and no attempt to correct for a core shift was made.

3.1. 3C 273

This famous quasar was the first to have its spectral redshift identified (Schmidt 1963; z=0.158; 1 mas = 3.6 pc) and has been studied extensively at all wavebands (Perry, Ward & Jones 1987 and references therein). VLBI studies of the parsec-scale jet at centimeter wavelengths reveal typical motions of 0.6–1.2 mas yr^{-1} and components with lifetimes that vary from $\sim$1 to over 13 years (Abraham et al. 1994; Zensus et al. 1990).

The first VLBI polarimetry was performed by Roberts et al. (1990) at 5 GHz (epoch 1984.78) who found: (1) a fractional polarization that increased steadily with distance from the core from 0.5 – 50%; (2) polarized intensity dominated by the western ends of the jet in contrast to the total intensity which is core-dominated; and (3) an electric vector position angle in the western part of the jet nearly orthogonal to the jet axis, but that changes more rapidly in the inner 10 mas. They assumed that the RM was identically 0 everywhere. They justified this assumption based on the fact that the integrated RM for the core measured with the VLA is RM = +5 radians m^{-2} (Rusk 1988), and the polarized flux density of the western jet contained over 40% of the VLA polarized flux density. In the inner jet Roberts et al. recognized that there may be significant departures in the RM from 0, and in fact used the deviations of the polarization angles from the jet axis at 5 GHz to infer a RM of 22000 $r^{-2.2}$ radians m^{-2}, which implies an RM of 140 radians m^{-2} at $r \sim 10$ mas.

Leppänen et al. (1995) were the first to make polarimetric observations of 3C 273 (epoch 1994.45) with VLBI at 22 GHz. They found: (1) less than 0.5% polarization in the core; (2) generally disjoint peaks between the total and polarized intensities; (3) an increase in fractional polarization with distance from the core; and (4) a roughly longitudinal magnetic field orientation in the inner 2 mas that becomes misaligned at larger core distances (in direct contrast to the finding of Roberts et al. (1990)). Again they assumed an identically 0 RM throughout.

In Fig. 1a I show an image of the polarized intensity overlaid on the total intensity image at 15 GHz. Rough agreement can be found in both total intensity and polarized structure with the images of Leppänen et al. (1995). I have therefore adopted their labeling of the components (F1–F7), although there is a difference of nearly 2.5 years between our observations and my lower resolution results in the blending of some of these components. The core (F7) is found to be weakly polarized at the level of ∼2% (see Table 3). This contrasts with the lower fractional core polarization seen by Leppänen et al. and by Roberts et al., but given the variable nature of radio cores this result is not surprising. The polarized flux density increases with distance from the core reaching 27% at a distance of 10.6 mas at component F1.

The change in polarization angle with wavelength in the western jet (component F1) can be well fit with a λ^2-law fit. The derived Faraday Rotation Measure between 8 and 15 GHz is 200 ± 30 radians m^{-2}, and between 5 and 8 GHz (at lower resolution) is 80 ± 20 radians m^{-2}. This is still larger than the +5 radians m^{-2} integrated RM found by Rusk, but this value will also be influenced by polarized flux density from more distant jet components not sampled by the VLBA. With increasing proximity to the core, the RM appears to increase (see Fig. 7), going up to 800 radians m^{-2} at the position of component F4/5. Note that a RM of 800 radians m^{-2} corresponds to a change in χ of 164° at 5 GHz! Failure to account for the RM may lead to gross mistakes in understanding the underlying magnetic field of the jet. At the core, the change in polarization angle with frequency is not well fit by a λ^2-law between 8 and 15 GHz. This could be caused by spectral-index effects and a blending of components within the synthesized beam (see §4.). The RM-corrected magnetic field orientation is shown in Fig. 8. Outside the core, the magnetic field runs parallel to the local jet direction.

3.2. 3C 279

This quasar (z=0.538, 1 mas = 7.3 pc) has the distinction of being the first in which superluminal motion was discovered (Whitney et al. 1971). It has since been the subject of intense VLBI monitoring programs (Unwin et al. 1998; Wehrle et al. 1996) which reveal components moving outward from the core with proper motions ranging from 0.15 to 0.5 mas/yr. The outermost component monitored at 22 and 43 GHz at $\sim$ 3.2 mas from the core at epoch 1997.07, is long-lived (> 13 years with no signs of fading) and has a velocity of $\sim$0.23 mas/yr (Unwin et al. 1997). There is also a stationary, long-lived, component (C5) 1 mas west of the core. 3C 279 is strong and violently variable from radio to γ-rays (Hartman et al. 1996).

Leppänen et al. (1995) report polarimetric observations of 3C 279 (epoch 1994.45) with the VLBA at 22 GHz. They found a low core polarization (<3%), but claim that the very nearby ($\sim$0.1 mas) component C7 has a much higher degree of polarization and accounts for most of the polarized emission at 22 GHz. They also find their outermost component (C4) to be strongly polarized (15%) with an electric vector position angle of $\sim$70°.

At 15 GHz and 2.5 $\times$ 1 mas resolution, the core and inner jet components, D+C7+C6, seen by Leppänen et al. are blended together. This component has a net fractional polarization of 4% (see Table 3), but still dominates the polarized emission from 3C 279. At 8 GHz the fractional polarization of this component drops somewhat to 2.5%, and there is a swing in polarization angle with λ^2 (see Fig. 2b and Fig. 7) that is well fit by a RM of -1240 ± 10 radians m^{-2}. In the jet component C4, just 3 mas (22 pc) distant the RM is -70 ± 10 radians m^{-2}, and there is no depolarization between 15 and 8 GHz – the fractional polarization is constant at $\sim$10% as expected for such a low RM. At frequencies of 5 GHz and below, the polarized emission from 3C 279 is dominated by component C4. The RM-corrected magnetic field orientation is shown in Fig. 8. Both the core and component C4 have magnetic field structure perpendicular to the jet direction.

It is worth noting that all of the properties of component C4 – its long-lived nature, strength, strong polarization, and small RM make 3C 279 a suitable polarization angle calibrator for VLBI observations. With a few snapshots of 3C 279 it should be feasible for observations between 5–43 GHz to image the source in I, Q and U, and use the known polarization angle of component C4 to correct for the instrumental R-L phase difference. At frequencies below 5 GHz observations using the VLBA alone will have difficulting separating component C4 from the core, but since C4 will dominate the polarization properties, it is probably safe to use it as an absolute polarization angle calibrator to frequencies as low as 2 GHz. Below that frequency more distant jet components may begin to influence the polarized flux.

3.3. 3C 345

This superluminal quasar (z=0.595, 1 mas = 7.6 pc) is a strong emitter from the radio to UV (Bregman et al. 1986). It exhibits blazar properties (Impey & Neugebauer 1988) and has a high optical polarization (Moore & Stockman 1984). 3C 345 has been extensively studied using VLBI (Unwin et al. 1983; Biretta, Moore, & Cohen 1986; Zensus, Cohen, & Unwin 1995) over distances ranging from 0.1 to 12 mas from the unresolved core.

Brown, Roberts & Wardle (1994) studied the milliarcsecond polarization structure of 3C 345 at 5 GHz and its evolution from 1981–1987. They found in general that the core was weakly polarized (2-4%) and that fractional polarization increased in components with distance from the core reaching a maximum of $\sim$15%. The electric vector position angle (assuming no Faraday Rotation) was found to be variable in the core, but generally perpendicular to the jet axis beyond 2 mas, even as the jet bends through 25°.

Leppänen et al. (1995) present 22 GHz polarimetry of the inner 1 mas of 3C 345. They identify an unresolved core (D) and two jet components C8 and C7 with polarizations of 3%, 8% and 4% respectively. Both D and C7 were found to have electric vectors nearly parallel to the jet axis ($\chi \sim 83°$), while C8 (in between) had a polarization angle of $-49°$. Leppänen et al. assumed that there was no appreciable Faraday Rotation at 22 GHz.

In my highest resolution 15 GHz image (see Fig. 3), I identify the core (D) and two jet components with perhaps another new jet component just emerging from the core. There is also a diffuse jet extending $\sim$18 mas which is better seen at 8 GHz (Fig. 4a). Given the very similar morphology of the inner jet to that seen by Leppänen et al., and the history of component motions at the level of 0.2-0.5 mas/yr (Zensus et al. 1995), I identify the two prominent jet components in our 15 GHz image with C7 and C8. I find that the polarization increases from 3.8% to 5.9% to 7.8% for the core, C8 and C7 respectively. The polarization angles measured, however, are quite different from those of epoch 1994.45 reported by Leppänen et al.. As evident in Fig. 3, both the core and C7 have polarization angles nearly perpendicular to the jet axis – 90° different from that reported by Leppänen et al.. Only component C8 has maintained a similar polarization angle at $-53°$. The observations are not at odds as variability of component polarization angles in 3C 345 is known to occur (Brown et al. 1994). Observations at 14.5 GHz by the University of Michigan Radio Astronomy Observatory (UMRAO) show a swing in the integrated polarization angle from $\sim$80° in 1994.4 to $\sim$14° in 1997.1. The same data show an increase in the fractional polarization from 1.7% (136 mJy) in 1994.4 to 4.0% (280 mJy) in 1997.1.

No significant Faraday rotation is found between 12 and 15 GHz in components D, C8 and C7, however these high-frequencies are only sensitive to RMs > 400 radians m^{-2}. Between 5 and 8 GHz at a resolution of 3.0×1.7 mas the "core" (really a blend of components D, C8 and C7), has an integrated RM of -130 ± 10 radians m^{-2} (Fig. 4b and Fig. 7). This will cause a rotation in χ of 27° at 5 GHz. In the jet the RM falls to -70 ± 35 radians m^{-2}. The RM-corrected magnetic field orientation, generally parallel to the local jet direction, is shown in Fig. 8.

3.4. 3C 380

This quasar (z=0.692, 1 mas = 7.9 pc) is among the most luminous sources in the 3C catalog. Although traditionally classified as a Compact Steep Spectrum source, it is more likely to be an FRII source viewed at a small angle to the line-of-sight (Wilkinson et al. 1991). The mas-scale structure and evolution has been studied by Polatidis & Wilkinson (1997) at frequencies ranging from 1.6 to 22 GHz. Polatidis & Wilkinson find dramatic changes in flux density and structure at the bright component (A) 8.9 mas northwest of the core at epoch 1997.07, and an average proper motion of 0.2 mas/yr.

The only polarimetric VLBI observation in the literature is reported by Cawthorne et al. (1993) for epoch 1984.78 at 5 GHz. Cawthorne et al. find the core component to be <1% polarized, and component A to be ∼4% polarized. Further from the core in the broad, extended jet, they find the polarization to increase to 77%, near the theoretical maximum permitted from incoherent synchrotron emission. Cawthorne et al. note that the electric field vectors in this extended jet are also remarkable in their uniformity – the projected magnetic field lies within 4° of the local jet direction after correction using the integrated RM of 130 radians m^{-2} (Wilkinson et al. 1991). A comparison between the VLBI observations of Cawthorne et al. and nearly contemporaneous VLA observations by Rusk (1988) suggest that the intermediate scale structure is ∼8% polarized and has a projected magnetic field that continues to run parallel to the jet.

The core is found to be only weakly polarized at all frequencies (see Table 3). At 15 GHz in the inner jet (components C1 and C2) the polarization increases to 2.2% and 5.8% respectively and reaches a maximum of 13% at component A (Fig. 5a). The electric vector position angle changes abruptly between the core, C1 and C2. In the core, the RMs are not well fit by a λ^2-law. Good fits to a λ^2-law are obtained in component C1 with observed values of -880 ± 50 radians m^{-2}. In component C2 the RMs fall abruptly to -30 ± 70 radians m^{-2} and remain low throughout the extended jet (see Fig. 7 and Table 3). The RM-corrected magnetic field orientation is shown in Fig. 8.

Given the low RMs found at component C2 and beyond, I have combined the data from all 4 frequencies between 4.6 and 5.1 GHz to produce the image shown in Fig. 6. In addition to increasing the sensitivity through additional data, this has the added advantage of improving the *uv*-coverage and hence the image fidelity. I find component A to be 12% polarized, but do not find the polarization to increase as dramatically in the diffuse extended jet as reported by Cawthorne et al.. Rather the polarization ranges from 5-35% with the maximum values occurring along the edge of the source. At the edges the high fractional polarization may result in part from errors in the total intensity image.

4. Discussion

Evidence is presented for high Faraday Rotation Measures (|RM| > 1000 radians m^{-2}) near the center of activity in 3 of 4 bright quasars (3C 273, 3C 279, and 3C 380 but not 3C 345 – see Table 3). The jets of all 3 of these quasars have |RM|s less than 100 radians m^{-2} beyond a projected distance from the nucleus of 20 h^{-1} pc – small enough to be produced by the passage of the radiation through the ISM of our Galaxy.

Sample fits to the RMs of the core show large deviations from a λ^2-law of rotation in 3C 273 and 3C 380. This could be due to effects that change the position angle of subcomponents within the core as a function of wavelength. This has been discussed by Wrobel (1987), Rudnick & Jones (1983), and O'Dea (1989) and their ideas are summarized here. Higher resolution observations have demonstrated that these "cores" have considerable substructure (e.g. Leppänen et al. 1995) consisting of the unresolved center of activity and recently emerged jet components. Several effects including (1) different intrinsic polarization angles, (2) relativistic aberration of subcomponents with the same intrinsic polarization angle, but different velocities, and (3) an RM gradient across the core, could all produce subcomponents with different polarization angles. Different synchrotron opacities or spectral indices between subcomponents could then cause them to exchange dominance with frequency within the core resulting in a dramatic change in polarization angle with frequency. These changes in polarization angle might be accompanied by depolarization, or even repolarization. In fact, a large range in depolarization is seen for the core components in Table 3. It is worthwhile to note that good fits to a λ^2-law are obtained for all the jet components, regardless of the magnitude of the RM, or their spectral index, perhaps because these components do not have as much substructure.

That the cores and inner jets of all three sources have high RMs (>2000) radians m^{-2} in their rest frame is strongly suggestive that the nuclear environment of quasars may be responsible for generating high RMs. This would also explain the lack of any correlation between the polarization angle of the core and source structure as previously suggested for 3C 273 by Roberts et al. (1990).

4.1. Origin of the High Central Rotation Measures

Internal Faraday rotation cannot produce the observed RMs since it also results in severe depolarization for rotations of 90° or more (Burn 1966). Similar conclusions were reached by Udomprasert et al. (1997) in considering the high RMs in the nuclear region of OQ 172.

Investigating the RM structure of the nuclear region of Quasars and Galaxies on the parsec scale may reveal a wealth of information about the densities and magnetic fields of the circumnuclear region since the RM measures the density weighted magnetic field along the line of sight:

$$RM = 812 \int_0^L n_{\rm e} B_{||} {\rm d}l \ \text{radians m}^{-2} \ , \tag{1}$$

where n_e is the electron density in cm^{-3}, $B_{||}$ is in mGauss, and l is in pc. On average the magnetic field, B, will be larger than the parallel component, $B_{||}$, by $\sqrt{3}$.

Two regions containing thermal gas which could act as a Faraday screen if magnetized are the broad line region (BLR) and the narrow line region (NLR) associated with active galactic nuclei. The BLR is thought to have a size of $\sim$ 0.1 pc and magnetic field strengths of perhaps 1 G (Rees 1987), however the region of high RM in 3C 273 and 3C 380 extends over 10–20 h^{-1}

pc. Thus the BLR is unlikely to produce coherent RMs on the observed scale. The NLR has been observed to cover a region of 100–1000 pc albeit with a small volume filling factor ($\epsilon \sim 10^{-3}$ [Osterbrock 1989]). In order to produce a coherent RM on scales of 10s of pc, the covering factor of the NLR must be close to unity, and the free-free opacity must be sufficiently low such that the radio source is not extinguished at centimeter wavelengths. Furthermore the magnetic fields must be organized on scales of >1 pc to avoid complete depolarization of the emission by differential Faraday rotation across the synthesized telescope beam. Free-free opacities for the NLR, with the standard estimates for density of 10^4 cm^{-3} and temperature of 10^4 K, are much less than unity at centimeter wavelengths (Ulvestad et al. 1981). The covering factor is not known, but it could be close to unity if the NLR clouds form preferentially in the vicinity of the radio jet (Norman & Miley 1984). Assuming a density of 10^4 cm^{-3}, and path length of 20 pc, the magnetic fields required to produce the RMs observed in 3C 273, 3C 279 and 3C 380 are 0.03, 0.03 and 0.07 μG respectively. These field strengths are much less than those needed to magnetically confine the NLR clouds.

4.2. Implications for Compact Steep Spectrum Sources

Based on low resolution observations, Compact Steep Spectrum (CSS) sources were found to comprise nearly half of the ∼15 sources then known to have rest frame RMs in excess of 700 radians m^{-2} (Taylor, Inoue & Tabara 1992). In a recent review of GPS (GHz Peaked Spectrum) and CSS sources, O'Dea (1998) found 12 of 37 (32%) of GPS/CSS sources to have rest frame RMs larger than 700 radians m^{-2}. Some researchers (e.g. Fanti 1990; Saikia et al. 1996) have interpreted similar evidence to indicate that CSS sources are embedded within a dense environment and are therefore likely to be confined (or frustrated), thus explaining their small size. High resolution observations of a CSS quasar known to have high RMs (OQ 172 – Udomprasert et al. 1996) reveal that the high RMs are produced only in the nuclear region, and are not indicative of a dense environment surrounding the entire source. Moreover, the discovery of similarly large RMs in the nuclear environments of typical (non-CSS) quasars like 3C 273 and 3C 279, indicates that the nuclear environments of these large sources are similar to those of the CSS quasars. High resolution RM observations of the CSS quasar 3C 309.1 by Aaron, Wardle, & Roberts (1998), reveal smooth and small RMs across this source. More high resolution RM observations are needed to determine the origin of the high RMs seen toward CSS and GPS sources.

The other class of sources known to exhibit high RMs are radio galaxies embedded in cooling flow clusters (Taylor, Barton & Ge 1994 and references therein). In these sources the high RMs are produced by kpc-scale cluster magnetic fields. By analogy the high RMs might be taken as evidence for a cluster environment around CSS/GPS sources. Supporting evidence from X-ray observations seems mixed (O'Dea 1998). Once again high resolution RM observations are needed to discriminate between a kpc-scale Faraday screen produced by cluster magnetic fields and a pc-scale Faraday screen produced in the nuclear region. Certainly cluster magnetic fields cannot produce the large RM gradients in OQ 172. And the presence of high RMs in sources like 3C 273 which is not in a cooling flow cluster, clearly demonstrates that there is more than one way to produce high RMs.

5. Conclusions

Rest frame Faraday Rotation Measures in excess of 2000 radians m^{-2} are found in the nuclear regions of 3 out of 4 strong quasars studied. In all cases the high RMs are confined to the nuclear region within a projected distance of 20 h^{-1} pc of the center of activity. These results are somewhat surprising given the small RMs derived by lower resolution observations ($<$50 radians m^{-2}), but are not completely unexpected since high nuclear RMs have also been reported in the CSS quasars OQ 172 (Udomprasert et al. 1997) and 3C 138 (Cotton et al. 1997). The high RMs seen in these sources, and perhaps in other CSS sources as well, probably originate in the same region that produces the narrow optical emission lines. The high RM gradients seen between the nuclear region and the extended jets cannot be produced by cluster or galactic scale magnetic fields. Nor are the high RMs likely to be the result of interactions of the jet with a dense environment since this would at least equally favor the production of high RMs in the outer parts of the jet.

Given the possibility of high RMs in the nuclear regions, more care should be exercised in the interpretation of magnetic fields orientations in these regions. The common practice of using an identically 0 RM, or the integrated RM to correct measurements of the electric vector polarization angle is quite likely to be a dangerous assumption in these inner regions. Beyond the inner 50 pc (projected distance) using the integrated RM would seem, on the basis of the observations presented here, to be fairly safe.

I thank Athol Kemball for many useful discussions about polarization calibration. I also thank an anonymous referee for several insightful suggestions. This research has made use of data from the University of Michigan Radio Astronomy Observatory which is supported by the National Science Foundation and by funds from the University of Michigan. This research has made use of the NASA/IPAC Extragalactic Database (NED) which is operated by the Jet Propulsion Laboratory, Caltech, under contract with NASA.

TABLE 1

VLBA Observational Parameters

Source (1)	Frequency (2)	BW (3)	Scans (4)	Time (5)
0814+425	4.616, 4.654, 4.854, 5.096	8	2	7
	8.114, 8.209, 8.369, 8.594	8	2	7
	12.115, 12.591	16	2	7
	15.165	32	2	7
1803+784	4.616, 4.654, 4.854, 5.096	8	2	7
	8.114, 8.209, 8.369, 8.594	8	2	10
	12.115, 12.591	16	2	7
	15.165	32	2	7
3C 273	4.616, 4.654, 4.854, 5.096	8	7	25
	8.114, 8.209, 8.369, 8.594	8	7	28
	12.115, 12.591	16	7	28
	15.165	32	7	28
3C 279	4.616, 4.654, 4.854, 5.096	8	7	35
	8.114, 8.209, 8.369, 8.594	8	7	29
	12.115, 12.591	16	7	29
	15.165	32	7	29
3C 345	4.616, 4.654, 4.854, 5.096	8	7	34
	8.114, 8.209, 8.369, 8.594	8	7	29
	12.115, 12.591	16	7	29
	15.165	32	7	29
3C 380	4.616, 4.654, 4.854, 5.096	8	7	33
	8.114, 8.209, 8.369, 8.594	8	7	29
	12.115, 12.591	16	7	29
	15.165	32	7	28

Notes to Table 1

Col.(1).—Source name. Col.(2).—Observing frequency in GHz. Col.(3).—Total spanned bandwidth in MHz. Col.(4).—Number of scans (each 2 – 4 minutes duration). Col.(5).—Total integration time on source in minutes.

TABLE 2

Polarization Angle Calibration

Source (1)	ν (2)	$S_{\rm VLA}$ (3)	$S_{\rm VLBA}$ (4)	$P_{\rm VLBA}$ (5)	$P_{\rm VLA}$ (6)	$\chi_{\rm VLA}$ (7)
0814+425	4.7	1.3	1.2	40	38	70
	8.4	1.4	1.5	29	35	79
	15.2	1.4	1.3	43	39	83
1803+784	4.7	2.5	2.7	65	97	62
	8.4	2.5	2.6	52	89	86
	15.2	2.6	2.3	64	84	−76

Notes to Table 2

Col.(1).—Source name. Col.(2).—Observing band in GHz. Col.(3).—Integrated VLA flux density in Jy. Col.(4).—Integrated VLBA flux density in Jy. Col.(5).—Integrated VLBA polarized flux density in mJy. Col.(6).—Integrated VLA polarized flux density in mJy. Col.(7).—VLA polarization angle (E-vector) in degrees.

TABLE 3

COMPONENT POSITIONS, FLUX DENSITIES, AND ROTATION MEASURES

Comp (1)	r (2)	I_{15} (3)	P_{15} (4)	m_{15} (5)	χ_{15} (6)	I_8 (7)	P_8 (8)	m_8 (9)	χ_8 (10)	RM (11)	B (12)	$D_{15/8}$ (13)
3C 273												
F6+F7	0.0	13500	30	2.2	42	9500	27	2.8	−2	−1900	48	0.8
F4+F5	2.4	2300	303	13	−38	2700	173	6.4	−10	500	41	2.1
F1	10.6	410	111	27	−65	680	180	26	−50	200	23	1.0
3C 279												
D+C7	0.0	17500	701	4.0	37	9100	224	2.5	−23	−1280	−21	1.6
C4	3.2	2500	265	11	72	2500	254	10	70	−64	−16	1.0
3C 345												
D+C8+C7	0.0	4920	167	3.4	−4	4220	62	1.5	−21	−130	78	2.3
jet	5.0	57	–	–	–	140	16	11	−2	−70	−87	–
3C 380												
core	0.0	1250	6.3	0.5	49	650	8.0	1.2	87	−2220	−24	0.4
C1	1.0	280	6.2	2.2	−34	260	9.5	3.7	−83	−880	72	0.6
C2	3.0	180	11	5.8	−4	210	4.1	2.0	−8	−26	86	2.9
A	8.9	110	15	13	7	110	15	13	7	4	−84	1.0

NOTES TO TABLE 3

Col.(1).—Component name. Col.(2).—Distance from the core in mas. Col.(3).—15.165 GHz total intensity in Jy/beam. Col.(4).—15.165 GHz polarized intensity in Jy/beam. Col.(5).—15.165 GHz fractional polarization in %. Col.(6).—15.165 GHz electric vector polarization angle in degrees. Col.(7).—8.369 GHz total intensity in Jy/beam. Col.(8).—8.369 GHz polarized intensity in Jy/beam. Col.(9).—8.369 GHz fractional polarization in %. Col.(10).—8.369 GHz electric vector polarization angle in degrees. Col.(11).—Observed Faraday Rotation Measure in rad m^{-2} derived from a linear least-squares fit to the polarization angle measurements between 8.114 and 15.165 MHz as discussed in the text. If generated in the rest frame of the source these values are larger by a factor of $(1+z)^2$. Col.(12).—Magnetic Field polarization angle corrected for RM. Col.(13).—Depolarization (m_{15}/m_8).

REFERENCES

Aaron, S. E., Wardle, J. F. C., & Roberts, D. H. 1998 in IAU Colloquium 164: Radio Emission from Galactic and Extragalactic Compact Sources, eds. J.A. Zensus, G.B. Taylor, and J. M. Wrobel, ASP Conference Series, Vol. 144, in press.

Abraham, Z., Carrara, E. A, Zensus, J. A & Unwin, S. C. 1994, in Compact Extragalactic Radio Sources, eds. J. A. Zensus & K. I. Kellermann (Green Bank: NRAO) 87–90.

Biretta, J. A., Moore, R. L., & Cohen, M. H. 1986, ApJ, 308, 93

Blandford, R. D., & Königl, A. 1979, ApJ, 232, 34

Brown, L. F., Roberts, D. H., & Wardle, J. F. C. 1994, ApJ, 437, 108

Bregman, J.N., et al. 1986, ApJ, 301, 708

Burn, B. F. 1966, MNRAS, 133, 67

Cawthorne, T. V., Wardle, J. F. C., Roberts, D. H., Gabuzda, D.C., & Brown, L. F. 1993, ApJ, 416, 496

Cotton, W. D. 1993, AJ, 106, 1241

Cotton, W. D., Fanti., C., Fanti, R., Dallacasa, D., Foley, A. R., Schilizzi, R. T., & Spencer, R. E. 1997, A&A, 325, 493

Fanti, R. 1990, in Proceedings of the Dwingeloo workshop on Compact Steep Spectrum and GHz Peaked Spectrum Radio Sources, eds C. Fanti, R. Fanti, C. P. O'Dea, and R. T. Schilizzi, (Istituto di Radioastronomia: Bologna), p. 218

Hartman, R. C., et al. 1996, ApJ, 461, 698

Impey, C. G., & Neugebauer, G. 1988, AJ, 95, 307

Lobanov, A. 1996, Ph.D. thesis, New Mexico Institute of Mining and Technology

Leppänen, K. J., Zensus, J. A., & Diamond, P. J. 1995, AJ, 110, 2479

Moore, R. L., & Stockman, H. S. 1984, ApJ, 279, 465

Norman, C., & Miley, G. 1984, ApJ, 141, 85

O'Dea, C. P. 1989, A&A, 210, 35

O'Dea, C. P. 1998, PASP, in press.

Osterbrock, D. E. 1989, Astrophysics of Gaseous Nebulae and Active Galactic Nuclei (Mill Valley: University Science Books)

Perry, J. J., Ward, M. J., & Jones, M. 1987, MNRAS, 228, 623

Polatidis, A. G., & Wilkinson, P. N. 1997, MNRAS, in press

Rees, M. J. 1987, MNRAS, 228, 47P

Roberts, D. H., Wardle, J. F. C., Brown, L. F., Gabuzda, D. C., & Cawthorne, T. V. 1989 in Parsec-Scale Radio Jets, eds. A. Zensus & T. Pearson, Cambridge, p.110

Roberts, D.H., Kollgaard, R.I., Brown, L.F., Gabuzda, D.C., & Wardle, J.F. 1990, ApJ 360, 408

Roberts, D. H., Wardle, J. F. C., & Brown, L. F. 1994, ApJ, 427, 718

Rudnick, L., & Jones, T. W. 1983, AJ, 88, 518

Rusk, R. 1988, Ph.D. thesis, University of Toronto

Saikia, D. J., Jeyakumar, S., Wiita, P. J., & Hooda, J. S. 1996, in Proceedings of the Second Workshop on Gigahertz Peaked Spectrum and Compact Steep Spectrum Radio Sources, eds I. A. G. Snellen, R. T. Schilizzi, H. J. A. Röttgering, & M. N. Bremer (Leiden: Leiden University Press), p. 252

Schmidt, M. 1963, Nature, 197, 1040

Schwab, F. R., & Cotton, W. D. 1983, AJ, 88, 688

Shepherd, M. C., Pearson, T. J., & Taylor, G. B. 1994, BAAS, 26, 987

Shepherd, M. C., Pearson, T. J., & Taylor, G. B. 1995, BAAS, 27, 903

Taylor, G. B., Inoue, M, & Tabara, H. 1992. A&A, 264, 421

Taylor, G. B., Barton, E. J., & Ge, J. 1994. AJ, 107, 1942

Udomprasert, P. S., Taylor, G.B., Pearson, T.J., & Roberts, D.H. 1997, ApJL, 483, L9

Ulvestad, J. S., Wilson, A. S., Sramek, R. A. 1981, ApJ, 247, 419

Unwin, S. C., Cohen, M. H., Pearson, T. J., Seielstad, G. A., Simon, R. S., Linfield, R. P., & Walker, R. C. 1983, ApJ, 271, 536

Unwin, S. C., Wehrle, A. E., Xu, W., Zook, A. C., & Marscher, A. P. 1998 in IAU Colloquium 164: Radio Emission from Galactic and Extragalactic Compact Sources, eds. J.A. Zensus, G.B. Taylor, and J. M. Wrobel, ASP Conference Series, Vol. 144, in press.

Wehrle, A. E., Unwin, S. C., Zook, A. C., Urry, C. M., Marscher, A. P., & Teräsranta, H. 1996, in Blazar Continuum Variability, eds. H. R. Miller, J. R. Webb & J. C. Noble, ASP Conference (San Francisco: Astron. Soc. of the Pacific), 430

Whitney, A. R., Shapiro, I. I., Rogers, A. E. E., Robertson, D. S., Knight, C. A., Clark, T. A., Goldstein, R. M., Marandino, G. E., & Vandenberg, N. R. 1971, Science, 173, 225

Wilkinson, P. N., Akujor, C. E., Cornwell, T. J., Saikia, D. J. 1991, MNRAS, 248, 86

Wrobel, J.M. 1987, in Superluminal Radio Sources, eds. J. A. Zensus & T. J. Pearson (Cambridge Univ. Press: Cambridge), p. 186

Zensus, J. A., Unwin, S. C., Cohen, M. H., & Biretta, J. A. 1990, AJ, 100, 1777

Zensus, J. A., Cohen, M. H., & Unwin, S. C. 1995, ApJ, 443, 35

This preprint was prepared with the AAS LaTeX macros v4.0.

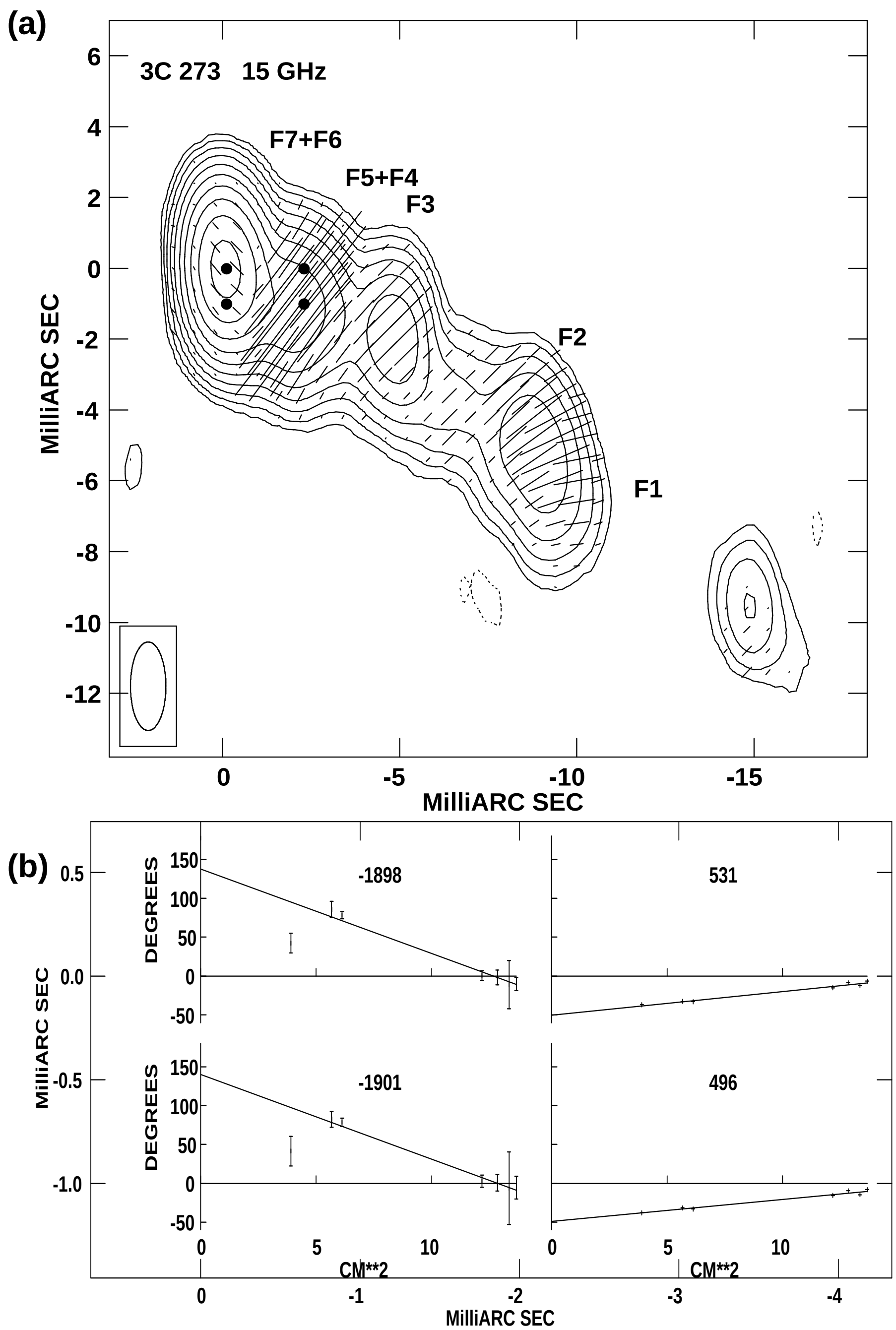

Fig. 1.— **(a)** Polarized intensity electric vectors (1 mas = 50 mJy/beam) overlaid on total intensity contours for 3C 273 at 15 GHz. Contours are plotted at −20, 20, 40, ... 10240 mJy/beam with negative contours shown dashed. The restoring beam is plotted in the lower left corner and has dimensions 2.5×1.0 mas in position angle 0°. The bullets (•) indicate representative points where the rotation measure fit has been plotted. **(b)** The electric vector position angle as a function of λ^2 between 8 and 15 GHz and the derived RM fits for the points shown in (a).

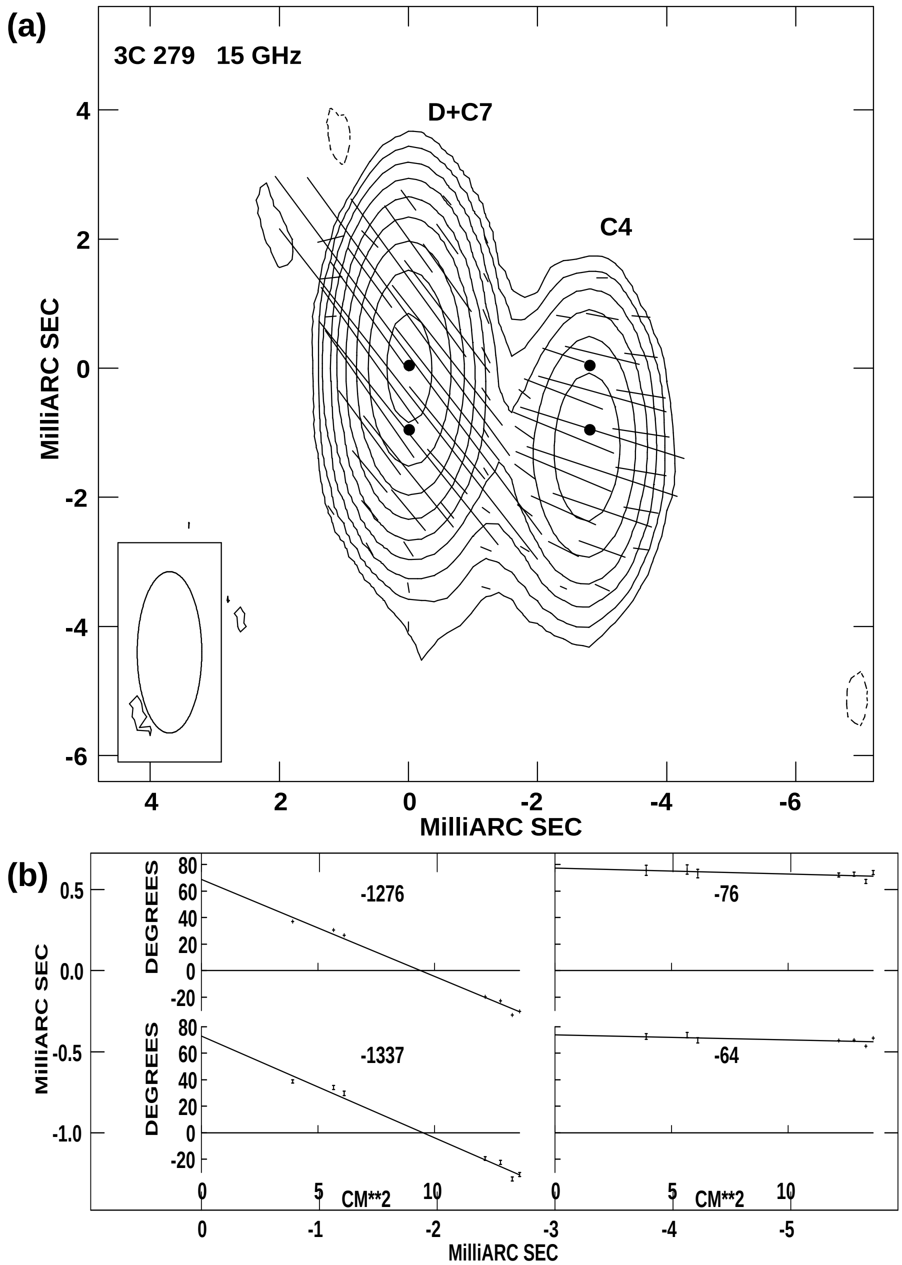

Fig. 2.— **(a)** Polarized intensity electric vectors (1 mas = 100 mJy/beam; vectors not corrected for Faraday rotation) overlaid on total intensity contours for 3C 279 at 15 GHz. Contours are plotted at −50, 50, 100, ... 10240 mJy/beam with negative contours shown dashed. The restoring beam is plotted in the lower left corner and has dimensions 2.5×1.0 mas in position angle 0°. The bullets (•) indicate representative points where the rotation measure fit has been plotted. **(b)** The electric vector position angle as a function of λ^2 between 8 and 15 GHz and the derived RM fits for the points shown in (a).

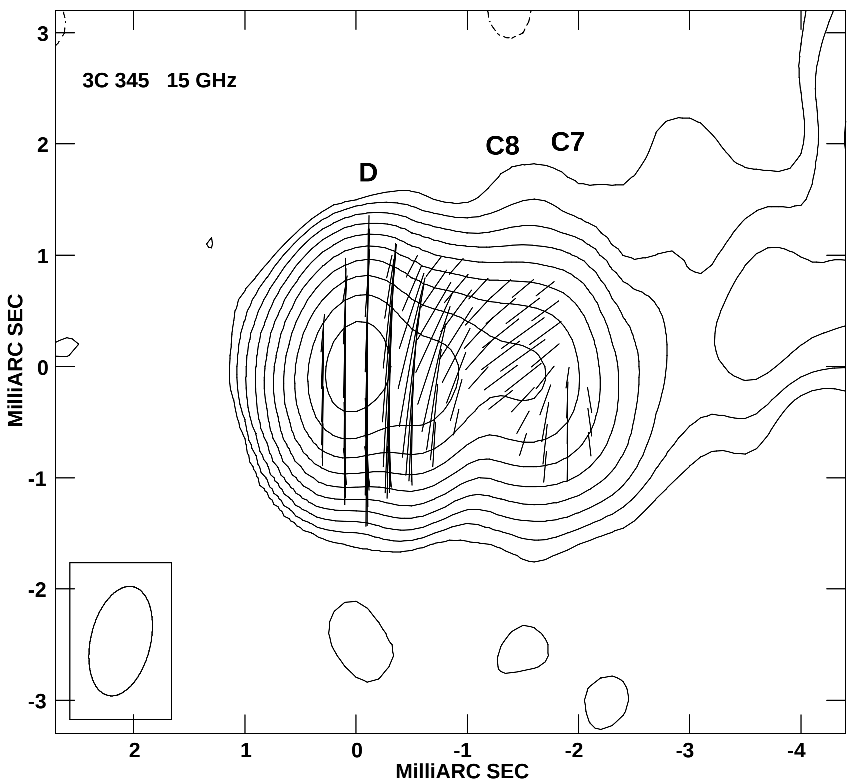

Fig. 3.— **(a)** Polarized intensity electric vectors (1 mas = 50 mJy/beam; vectors not corrected for Faraday rotation) overlaid on total intensity contours for the inner core and jet of 3C 345 at 15 GHz. Contours are plotted at -4, 4, 8, ... 2048 mJy/beam with negative contours shown dashed. The restoring beam is plotted in the lower left corner and has dimensions 1.0×0.54 mas in position angle $-13°$.

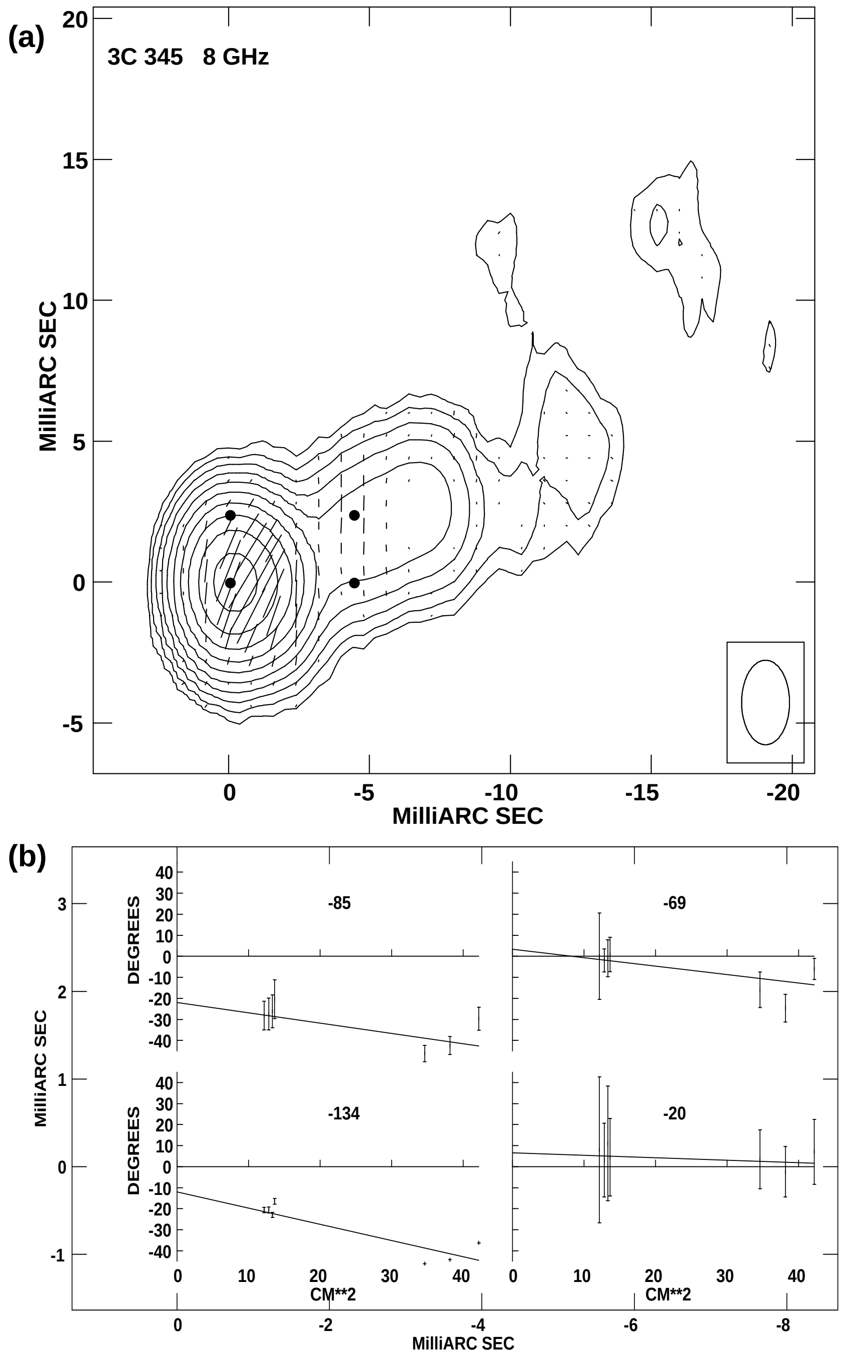

Fig. 4.— **(a)** Polarized intensity electric vectors (1 mas = 25 mJy/beam; vectors not corrected for Faraday rotation) overlaid on total intensity contours for 3C 345 at 8 GHz. Contours are plotted at −6, 6, 12, ... 3072 mJy/beam with negative contours shown dashed. The restoring beam is plotted in the lower left corner and has dimensions 3.0 × 1.7 mas in position angle 0°. The bullets (•) indicate representative points where the rotation measure fit has been plotted. **(b)** The electric vector position angle as a function of λ^2 between 5 and 8 GHz and the derived RM fits for the points shown in (a).

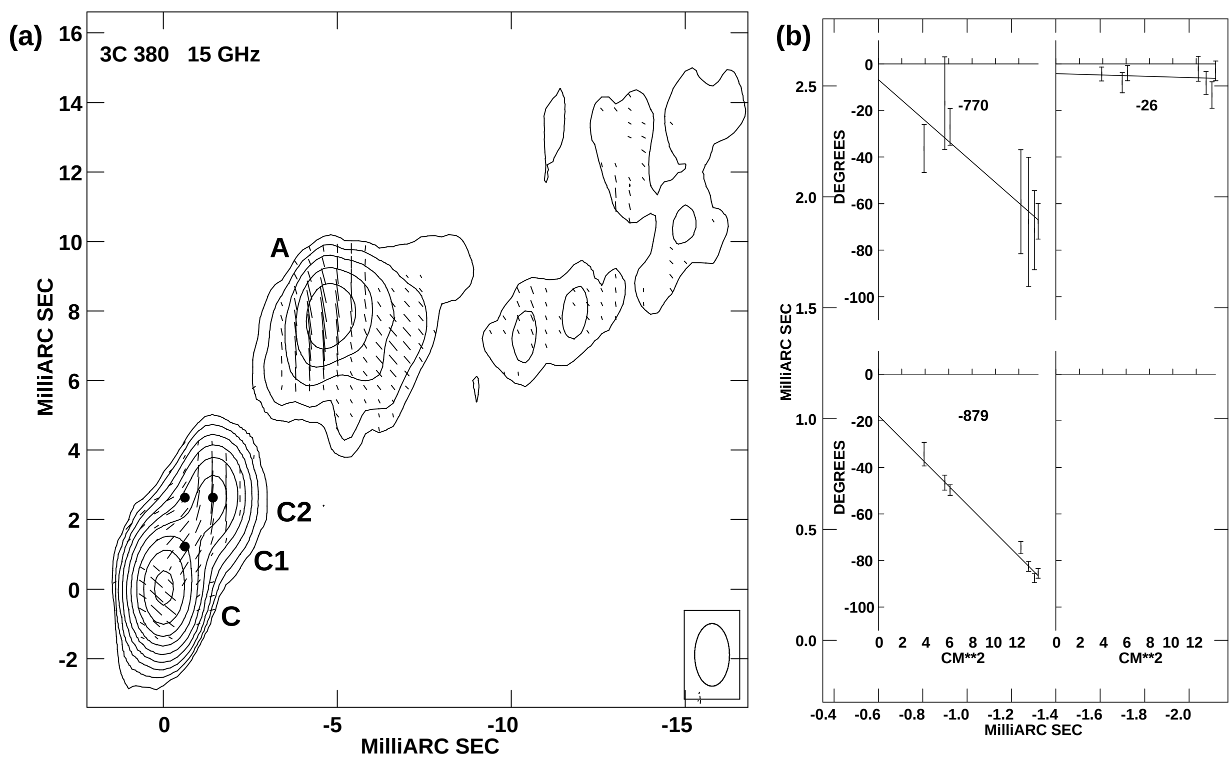

Fig. 5.— **(a)** Polarized intensity electric vectors (1 mas = 13 mJy/beam; vectors not corrected for Faraday rotation) overlaid on total intensity contours for 3C 380 at 15 GHz. Contours are plotted at −4, 4, 8, ... 1024 mJy/beam with negative contours shown dashed. The restoring beam is plotted in the lower left corner and has dimensions 1.8 × 1.0 mas in position angle 0°. The bullets (•) indicate representative points where the rotation measure fit has been plotted. **(b)** The electric vector position angle as a function of λ^2 between 8 and 15 GHz and the derived RM fits for the points shown in (a).

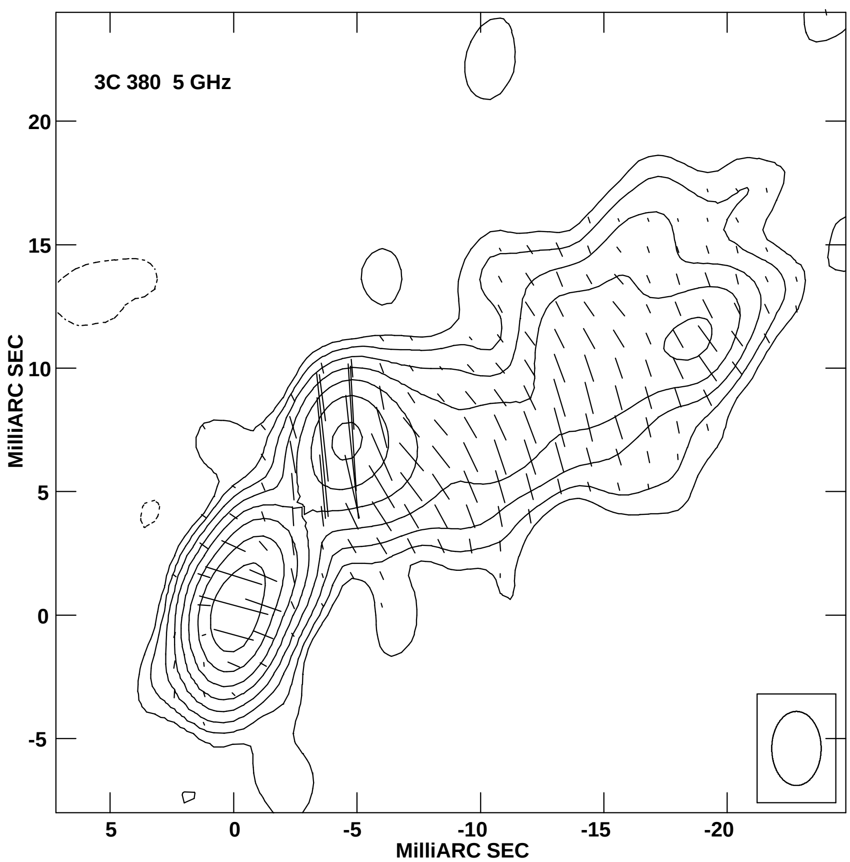

Fig. 6.— **(a)** Polarized intensity electric vectors (1 mas = 6.25 mJy/beam; vectors not corrected for Faraday rotation) overlaid on total intensity contours for 3C 380 at 5 GHz. Contours are plotted at -4, 4, 8, ... 512 mJy/beam with negative contours shown dashed. The restoring beam is plotted in the lower left corner and has dimensions 3×2 mas in position angle 0°.

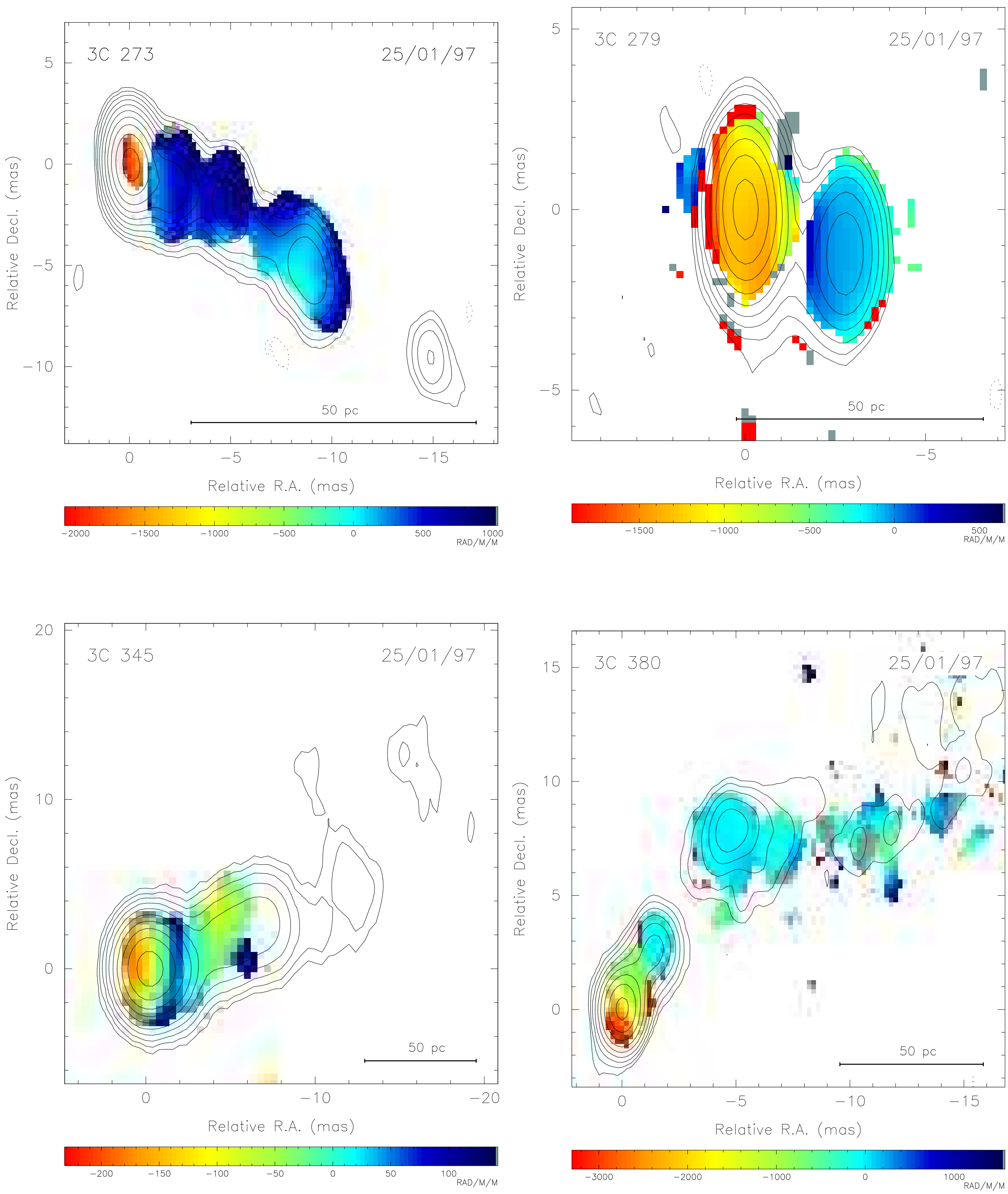

Fig. 7.— Rotation measure images of 3C 273, 3C 279, 3C 345, and 3C 380 with contours of total intensity superimposed. Contours are as in Figures 1, 2, 4, and 5.

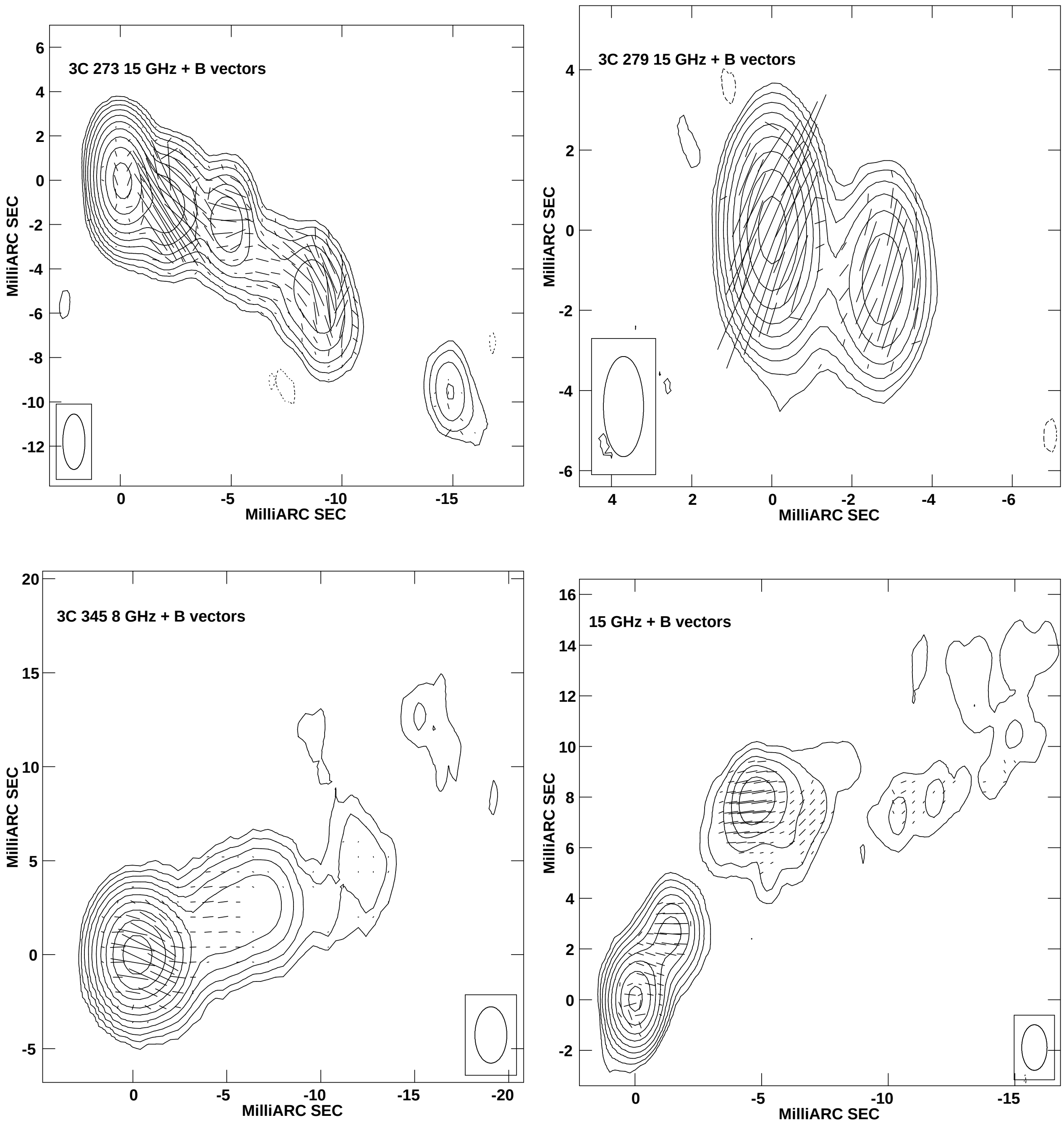

Fig. 8.— Projected magnetic field vectors (corrected for the RMs shown in Fig. 7) for 3C 273, 3C 279, 3C 345, and 3C 380 with contours of total intensity superimposed. Contours are as in Figures 1, 2, 4, and 5.